

# Optimized CO<sub>2</sub> Capture of the Zeolitic Imidazolate Framework ZIF-8 Modified by Solvent-Assisted Ligand Exchange

Yuel W. Abraha, Chih-Wei Tsai, J. W. Hans Niemantsverdriet, and Ernst H. G. Langner\*

Cite This: *ACS Omega* 2021, 6, 21850–21860

Read Online

ACCESS |



Metrics &amp; More

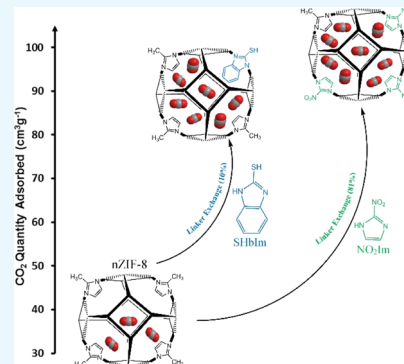


Article Recommendations



Supporting Information

**ABSTRACT:** Zeolitic imidazolate frameworks, like ZIF-8 and related structures, have shown great potential for the capture of carbon dioxide. Modifying their structure by exchanging part of the constituent organic ligands is a proven method for enhancing the capacity to absorb CO<sub>2</sub>. In this work, we performed solvent-assisted ligand exchange (SALE) on nanosized ZIF-8 (nZIF-8) with a series of functionalized imidazole derivatives (exchange percentages, after 24 h): 2-bromoimidazole (19%), 2-chloroimidazole (29%), 2-trifluoromethylbenzimidazole (4%), 2-mercaptobenzimidazole (4%), and 2-nitroimidazole (54%). The sodalite topology and porosity of nZIF-8 were maintained with all SALE modifications. Low-pressure CO<sub>2</sub> adsorption of nZIF-8 (38.5 cm<sup>3</sup> g<sup>-1</sup>) at STP was appreciably enhanced with all mixed-linker SALE products. Using halogenated (–Cl, –Br, and –CF<sub>3</sub>) imidazole derivatives in a 24 h SALE treatment resulted in increases between 11 and 22% in CO<sub>2</sub> adsorption, while the thiol (–SH)- and nitro (–NO<sub>2</sub>)-functionalized SALE products led to 32 and 100% increases in CO<sub>2</sub> uptakes, respectively. These CO<sub>2</sub> uptakes were further optimized by varying the SALE treatment time. The SHIm- and NO<sub>2</sub>Im-exchanged SALE products of nZIF-8 show 87 and 98 cm<sup>3</sup> g<sup>-1</sup> of CO<sub>2</sub> uptakes after 60 and 120 h of SALE, respectively. These are record high CO<sub>2</sub> adsorptions for all reported ZIF derivatives at low-pressure conditions.



## 1. INTRODUCTION

The removal of carbon dioxide (CO<sub>2</sub>), a major greenhouse gas from the atmosphere, has become one of the greatest environmental challenges faced by the human race in the 21st century.<sup>1–3</sup> At the time of writing, the level of CO<sub>2</sub> amounted to 415 ppm, which is about 100 ppm higher than in 1960 and predicted to grow further in the next 20 years due to the persistent usage of fossil fuels as the main source of energy.<sup>4</sup> CO<sub>2</sub> capture and storage/sequestration (CCS) technologies are considered essential as a short to mid-term solution to minimize the impact of global warming, up until renewable technologies reach the required maturity.<sup>5</sup>

Porous materials such as zeolites, bituminous coal-based activated carbon (BPL carbon), and metal–organic frameworks (MOFs) are being investigated for their high CO<sub>2</sub> adsorption capacities. In the last two decades, MOFs have attracted extensive attention for CCS applications owing to their high surface area, tunable pore size, high CO<sub>2</sub> selectivity, capacity, porosity, and thermal and chemical stabilities.<sup>3,6</sup> Zeolitic imidazolate frameworks (ZIFs) are a subclass of MOFs made of bivalent metal centers, tetrahedrally coordinated to imidazolate organic linkers. ZIFs have shown a high affinity for CO<sub>2</sub> over other components in flue gas resulting from fossil fuel combustion. This, coupled with independence on regeneration temperature, makes ZIFs ideal for industrial CO<sub>2</sub> uptake.<sup>7</sup>

Direct synthesis (*de novo*) of ZIFs with the desired linker (functionalized imidazole) and metal center combination

suffers from many limitations such as low solubility of linkers or metal salts, catenation, loss of porosity, formation of undesired topologies, and loss of sensitivity.<sup>8</sup> Solvent-assisted ligand/linker exchange (SALE) can be used to overcome these limitations. SALE, also known as a bridging-linker replacement, is a type of postsynthetic modification (PSM) where the organic linkers of a MOF are exchanged with another suitable linker in an appropriate solvent medium.<sup>9</sup> This is a heterogeneous reaction, where the parent MOF crystals are reacted with an excess of the new linkers. SALE occurs *via* single-crystal to single-crystal transformations as opposed to the dissolution of the framework and recrystallization.<sup>10</sup>

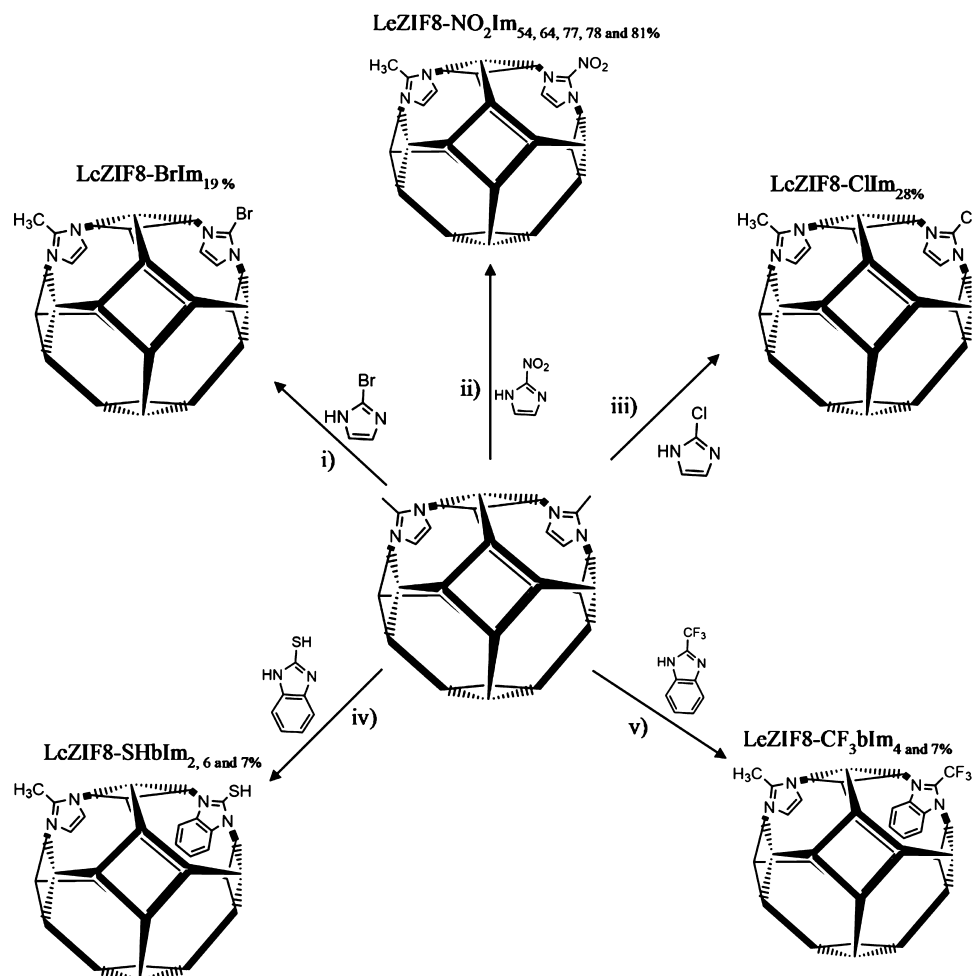
The term SALE was established by Karagiari *et al.*,<sup>11</sup> who used the method to replace the 2-ethylimidazole linkers of cadmium-based ZIF (CdIF-4) with 2-nitroimidazole (NO<sub>2</sub>Im) and 2-methylimidazole (mIm) in dimethylformamide (DMF), dimethylacetamide, and *n*-butanol solvents, resulting in the formation of CdIF-9 and SALEM-1, respectively. The RHO topology of the parent CdIF-4 was maintained in both SALE products. Furthermore, the particle size of the MOF remained

Received: March 2, 2021

Accepted: July 27, 2021

Published: August 18, 2021



Scheme 1. Summary of all SALE Reactions Used on ZIF-8 in This Study<sup>a</sup>

<sup>a</sup>Reaction conditions: (i) methanol, 60 °C, 24 h, (ii) methanol/DMF (1:1), 60 °C, 24–120 h, (iii) methanol, 60 °C, 24 h, (iv) *n*-butanol, 100 °C, 24–60 h, and (v) methanol, 60 °C, 24–168 h. Exchange percentages (as determined by <sup>1</sup>H NMR) are given as subscripts.

the same, while a high Brunauer–Emmett–Teller (BET) surface area was maintained.<sup>11</sup> The required molar ratio of imidazole linker to ZIF-8 was found to be 6.7:1, while the ratio 3:1 was adequate for performing SALE on CdIF-4. Higher molar ratios (>6.7:1) resulted in degradation of the framework, while lower molar ratios (<3:1) did not result in any ligand exchange.<sup>11</sup>

SALE can be selective when applied to mixed-linker MOFs. Lalonde *et al.* reported selective SALE of ZIF-69 (NO<sub>2</sub>Im and 5-ClbIm linkers), ZIF-78 (NO<sub>2</sub>Im and NO<sub>2</sub>bIm linkers), and ZIF-76 (Im and 5-ClbIm linkers) with 5-trifluorobenzimidazole.<sup>12</sup> The SALE was selective to the bulky linkers (5-ClbIm and NO<sub>2</sub>bIm), while the imidazole linkers remained unchanged. Linker exchanges of over 90% was achieved for all three ZIFs as determined by digestive <sup>1</sup>H nuclear magnetic resonance (NMR). Powder X-ray diffraction (PXRD) and N<sub>2</sub> adsorptions showed that the topology and permanent porosity of the ZIFs were retained during the ligand exchange. The selectivity of the SALE was directed by the pK<sub>a</sub> of the linkers as well as kinetic and steric factors. Similarly, Tuleushov and Attfield have shown that Zn(Im) (bIm) can be formed *via* selective SALE of 5-chlorobenzimidazole (5-ClbIm) linkers of ZIF-76 with benzimidazole at 100 °C over 5 days.<sup>8</sup> The selectivity was due to the similar pK<sub>a</sub> of 5-ClbIm (~5.74) and bIm (~5.74) compared to 14.5 of Im. The SALE product

maintained the LTA topology of the mother MOF according to PXRD analysis as well as scanning electron microscopy images.

The electronic and chemical properties of a MOF can be modified by SALE, introducing linkers with desired functional groups. SALE of ZIF-71 (Zn(dcIm)<sub>2</sub>) and ZIF-8 with 4-bromoimidazole and 2-ethyl-imidazole, respectively, resulted in the formation of ZIF-71(4-BrIm/dcIm) and ZIF-8 (mIm/eIm), both retaining the RHO and sodalite (SOD) topology of the parent MOFs, respectively.<sup>13,14</sup> Ban *et al.* have reported SALE of ZIF-108, Zn(NO<sub>2</sub>Im), with an exchange percentage for mIm (56%), eIm (40%), Im (12.5%), NO<sub>2</sub>bIm (50%), and dMebIm (20%) to form ZIF-108-mIm, ZIF-108-eIm, ZIF-70, ZIF-78, and ZIF-74, respectively.<sup>15</sup> ZIF-108-mIm and ZIF-108-eIm maintained the SOD topology of ZIF-108, while ZIF 70 & 78 resulted in GME topology, and ZIF-74 formed in GIS topology. The formation of different topologies is possible due to the heterogeneous nucleation process that takes place during SALE, where the parent ZIF acts as a seed.

During solvent-assisted ligand incorporation (SALI), another route for PSM of MOFs, the desired functionalities are incorporated into the MOF nodes. The CO<sub>2</sub> uptake of NU-1000 was enhanced by incorporating a perfluoroalkane functionality *via* SALI.<sup>16</sup> The SALI-1 product with

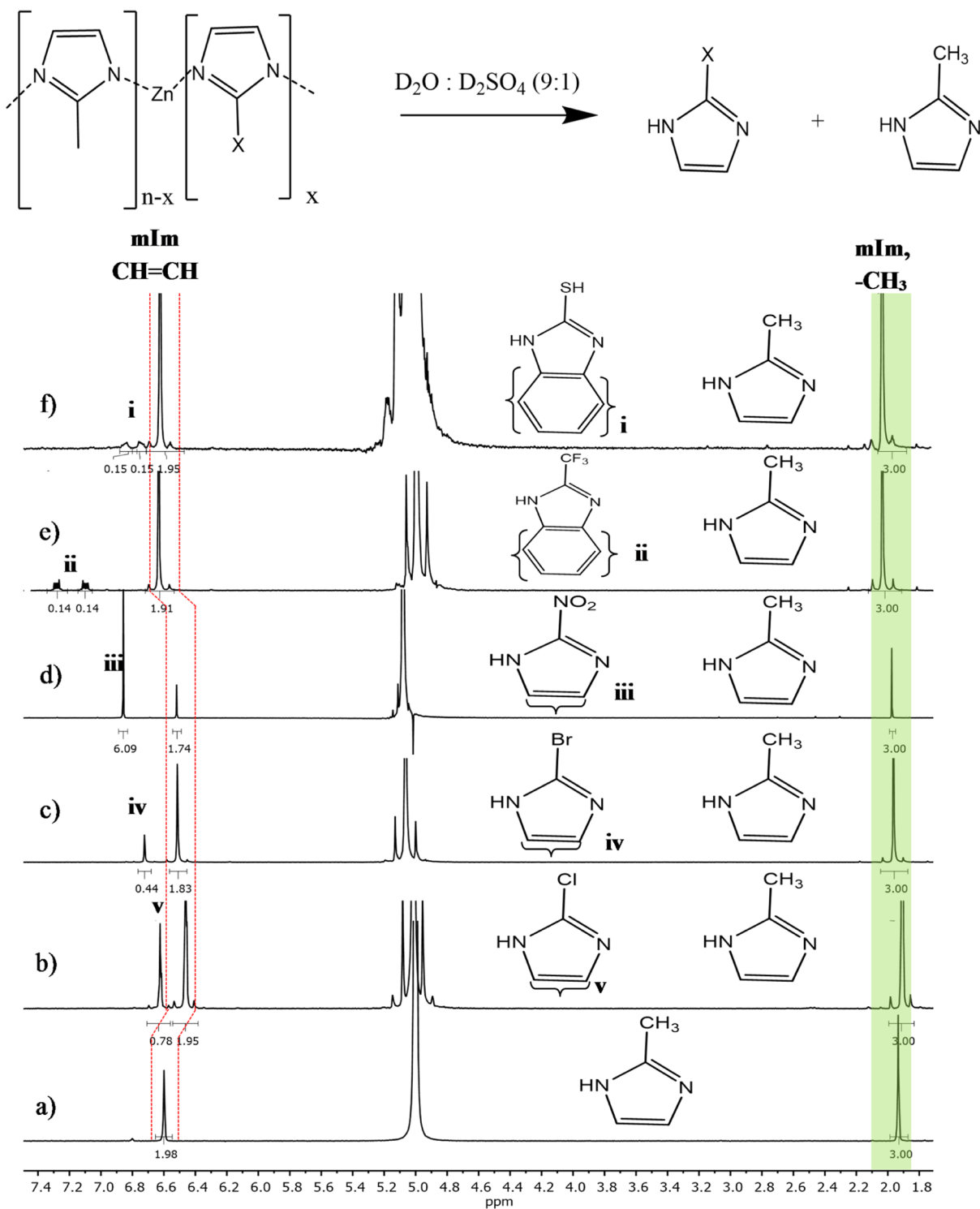


**Figure 1.**  $^1\text{H}$  digestive NMR spectra of (a) nZIF8, (b) LeZIF8-ClIm<sub>24h</sub>, (c) LeZIF8-BrIm<sub>24h</sub>, (d) LeZIF8-NO<sub>2</sub>Im<sub>96h</sub>, (e) LeZIF8-CF<sub>3</sub>bIm<sub>24h</sub>, and (f) LeZIF8-SHbIm<sub>60h</sub>.

CF<sub>3</sub>COO– functionality resulted in a 68% increase in CO<sub>2</sub> uptake at low pressure (0.15 bar) over the parent NU-1000.

Dual-linker ZIFs have shown enhanced selectivity for CO<sub>2</sub> than for other gases (CH<sub>4</sub>, O<sub>2</sub>, and N<sub>2</sub>) commonly found in flue gas.<sup>17</sup> Additionally, ZIFs with electron-withdrawing linkers exhibit improved CO<sub>2</sub> uptakes as a result of the enhanced interaction with CO<sub>2</sub>.<sup>18</sup> Yaghi and co-workers synthesized a series of ZIF 68–70 and ZIF 78–82 using *de novo* (conventional direct) method starting with a mixed-linker

system.<sup>17</sup> The ZIFs showed GME topology with a pore diameter of 16 Å. Increasing CO<sub>2</sub> adsorptions (at 1 bar) were observed with increasing electronegativity of the imidazole/benzimidazole linker's functionalities: ZIF-78 (–NO<sub>2</sub>, –NO<sub>2</sub>) > ZIF-69 (–NO<sub>2</sub>, –Cl), ZIF-81 (–NO<sub>2</sub>, –Br), ZIF-82 (–CN, –Cl) > ZIF-68 (–NO<sub>2</sub>, –H), > ZIF-70 (NO<sub>2</sub>, –H) > ZIF-79 (–NO<sub>2</sub>, –Me).<sup>17,19,20</sup> This is due to the high quadrupole moment of CO<sub>2</sub>. ZIFs with high quadrupole moments (ZIF-78 & 82) resulted in high adsorption as a result

of the increased interaction between CO<sub>2</sub> and the polar functional groups of the MOFs. No relations were found between the pore diameter and CO<sub>2</sub> adsorptions, which indicate that CO<sub>2</sub> adsorption is predominantly influenced by the functionalities of the linkers rather than the pore properties of the MOFs. Furthermore, ZIF-68, -69, -70, -78, -81, and -82 gave better CO<sub>2</sub> uptake (>55 cm<sup>3</sup> g<sup>-1</sup>) than the industrially used BPL carbon (46.8 cm<sup>3</sup> g<sup>-1</sup>).<sup>20</sup>

SALE can also be used to synthesize single-linker MOFs by complete exchange of the original linker with the linker of choice. TMU-4-SALE-L6 and TMU-4-SALE-L6 was obtained after SALE of TMU-4 and TMU-6, respectively. In both cases, complete linker exchange was achieved by an extended SALE time of 5 days at 80 and 100 °C, respectively.<sup>21</sup> The SALE products showed 10 and 30× increases in porosity over their *de novo* synthesized counterparts (TMU-4 and TMU-6). The CO<sub>2</sub> uptake (at 273 K and 1 bar) of TMU-4-SALE-L6 was doubled compared to that of the directly synthesized TMU-6.

In 2018, we reported a series of SALE products of nano-sized ZIF-8 (abbreviated as nZIF-8) with 2-mercaptobenzimidazole (SHbIm), 2-aminobenzimidazole (NH<sub>2</sub>bIm), 2-phenylimidazole (PhIm), and 2-nitroimidazole (NO<sub>2</sub>Im) with 12.5, 16, 10, and 67% linker exchanges, respectively.<sup>22</sup> SALE generally resulted in a decrease in the BET surface area of the ZIF, especially with the 2-nitroimidazole-exchanged ZIF, which has a BET surface area of 633 m<sup>2</sup> g<sup>-1</sup> compared to the 1605 m<sup>2</sup> g<sup>-1</sup> of parent nZIF-8. All of the nZIF-8 derivatives maintained the SOD topology of ZIF-8, while the NO<sub>2</sub>Im-exchanged SALE products developed an FRL topology. All SALE-modified ZIFs resulted in improved low-pressure CO<sub>2</sub> adsorptions at 0 °C, and ZIFs with electron-withdrawing (–NO<sub>2</sub> and SH) functionalities showed the highest CO<sub>2</sub> adsorptions of 76 and 77 cm<sup>3</sup> g<sup>-1</sup>, respectively. NO<sub>2</sub>Im-exchanged ZIF-8 showed considerably higher CO<sub>2</sub> adsorptions with half the BET surface area of its SH-functionalized (1416 cm<sup>3</sup> g<sup>-1</sup>) counterpart. Furthermore, an increase in CO<sub>2</sub> adsorption was observed with increasing electronegativity of the functional groups (NO<sub>2</sub> > SH > NH<sub>2</sub> > phenyl).<sup>22</sup>

Herein, we further explore the usefulness of the SALE method applied to nZIF-8 with 2-bromoimidazole (BrIm), 2-chloroimidazole (ClIm), and 2-trifluoromethylbenzimidazole (CF<sub>3</sub>bIm) linkers. We also aim to optimize the CO<sub>2</sub> uptake capacity under ambient conditions of the high-performing SALE products (with NO<sub>2</sub>Im and SHbIm linkers) of nZIF-8 by performing time-resolved SALE reactions.<sup>22</sup> We found that the SHbIm and NO<sub>2</sub>Im exchanged materials have CO<sub>2</sub> uptakes that are up to 2.5 times that of the parent ZIF-8, which are record high CO<sub>2</sub> adsorptions of all reported ZIF derivatives under ambient conditions.

## 2. RESULTS AND DISCUSSION

**2.1. Synthesis.** SALE was performed by isothermal heating of nZIF-8 suspended in methanol with ~3× excess of imidazolate-based linkers (ClIm, BrIm, or NO<sub>2</sub>Im) and ~8× excess of benzimidazolate-based linkers (SHbIm or CF<sub>3</sub>bIm) for the above stated reaction temperature and time (Scheme 1, Table 3). The mixed-linker ZIF products are denoted with a “Le” (ligand exchange) prefix, followed by “ZIF8” and a new linker name with SALE time and linker exchange percentages (as determined by <sup>1</sup>H NMR) as a subscript.

The ClIm, BrIm, and CF<sub>3</sub>bIm linkers were all dissolved in methanol prior to mixing with the suspended nZIF-8, while SHbIm was dissolved in 1-butanol and NO<sub>2</sub>Im in DMF due to

their low solubility in methanol. A minimum yield of 79% was achieved for all SALE reactions, with the exception of the LeZIF8-SHbIm products, which resulted in ~30% yields due to partial digestion of the nZIF-8 structure by the acidic thiol substituent.<sup>22</sup>

All SALE products were activated at 150 °C (in a vacuum oven overnight) to remove any solvents and unreacted linkers from the pores of the MOF. The mixed-linker SALE products were all stable under atmospheric conditions and thermally stable up to 264 °C in the N<sub>2</sub> atmosphere according to thermal gravimetric analysis (TGA) (Supporting Information Figure S10).

**2.2. Characterization.** **2.2.1. Digestive <sup>1</sup>H NMR.** Digestive <sup>1</sup>H NMR using the D<sub>2</sub>O/D<sub>2</sub>SO<sub>4</sub> (9:1) solvent system was used for quantitative determination of exchange percentages for the SALE products from the ratio of the integrals (or intensities) of CH=CH peaks of mIm and CH=CH or benzylic peaks (i–iv) of the new linkers (Figure 1, Table 3). The NO<sub>2</sub>Im, ClIm, and BrIm nZIF8-SALE products all have a singlet at ~1.82 ppm representing –CH<sub>3</sub> and another singlet at ~6.48 ppm corresponding to CH=CH of mIm protons. Additional peaks corresponding to CH=CH and benzylic protons of the new imidazole-based linkers are also observed between 6.6 and 7.4 ppm. The SHbIm and CF<sub>3</sub>bIm nZIF8-SALE products both lead to a downfield shift of the –CH<sub>3</sub> (mIm) peak to resonate at 1.92 and 1.98 ppm and CH=CH peak shift to 6.59 and 6.66 ppm, respectively. The shift is induced by the electron-withdrawing substituents (–CF<sub>3</sub> and –SH) forming intermolecular interactions with mIm protons in solution, for example, –H–S– or –H–F–. The benzylic ring could add a stabilizing effect to the intermolecular interactions in these two cases.

Nitro-functionalized SALE products (LeZIF8-NO<sub>2</sub>Im) were the least soluble in the used digestive system and required heating to achieve complete solubility. Thus, digestive NMR was only used as a preliminary method for linker exchange determination for the nitro-functionalized SALE products. LeZIF8-NO<sub>2</sub>Im shows the highest linker exchange (~55%) after 24 h compared to LeZIF8-ClIm<sub>24h</sub> (29%), LeZIF8-BrIm<sub>24h</sub> (19%), LeZIF8-CF<sub>3</sub>bIm<sub>24h</sub> (4%), and LeZIF8-SHbIm<sub>24h</sub> (2%). CF<sub>3</sub>bIm and SHbIm SALE products gave low exchange percentages (<10%) due to their bulky size, limiting the exchange to only the surface of nZIF-8. Thus, NO<sub>2</sub>Im is the most suited ligand for SALE of ZIF-8.

The linker exchanges of LeZIF8-SHbIm and LeZIF8-NO<sub>2</sub>Im products were further increased by time-resolved SALE reactions of 24–60 and 24–120 h, respectively. The effect of increasing the reaction time on the linker exchange of nZIF-8 with SHIm and NO<sub>2</sub>Im is observed as a relative decrease in the amount of mIm protons and an increase in the number of SHIm and NO<sub>2</sub>Im (Supporting Information Figures S7 and S8). The linker exchange rates for 2-mercaptobenzimidazole and 2-nitroimidazole both increased with time, reaching a maximum exchange of 7.2 and 81% after 60 and 120 h, respectively.

The digestive <sup>1</sup>H NMR spectrum of LeZIF8-SHbIm (Figure 1f; Supporting Information Figure S8) shows an overlap of the benzylic protons of the SHbIm linker (marked i) with the spinning sidebands of the CH=CH singlet of mIm. This overlap could cause the calculated exchange percentages to be lower than expected. Thus, the exchange percentages of the LeZIF8-SHbIm products were further verified using inductively coupled plasma (ICP), which indeed showed a higher

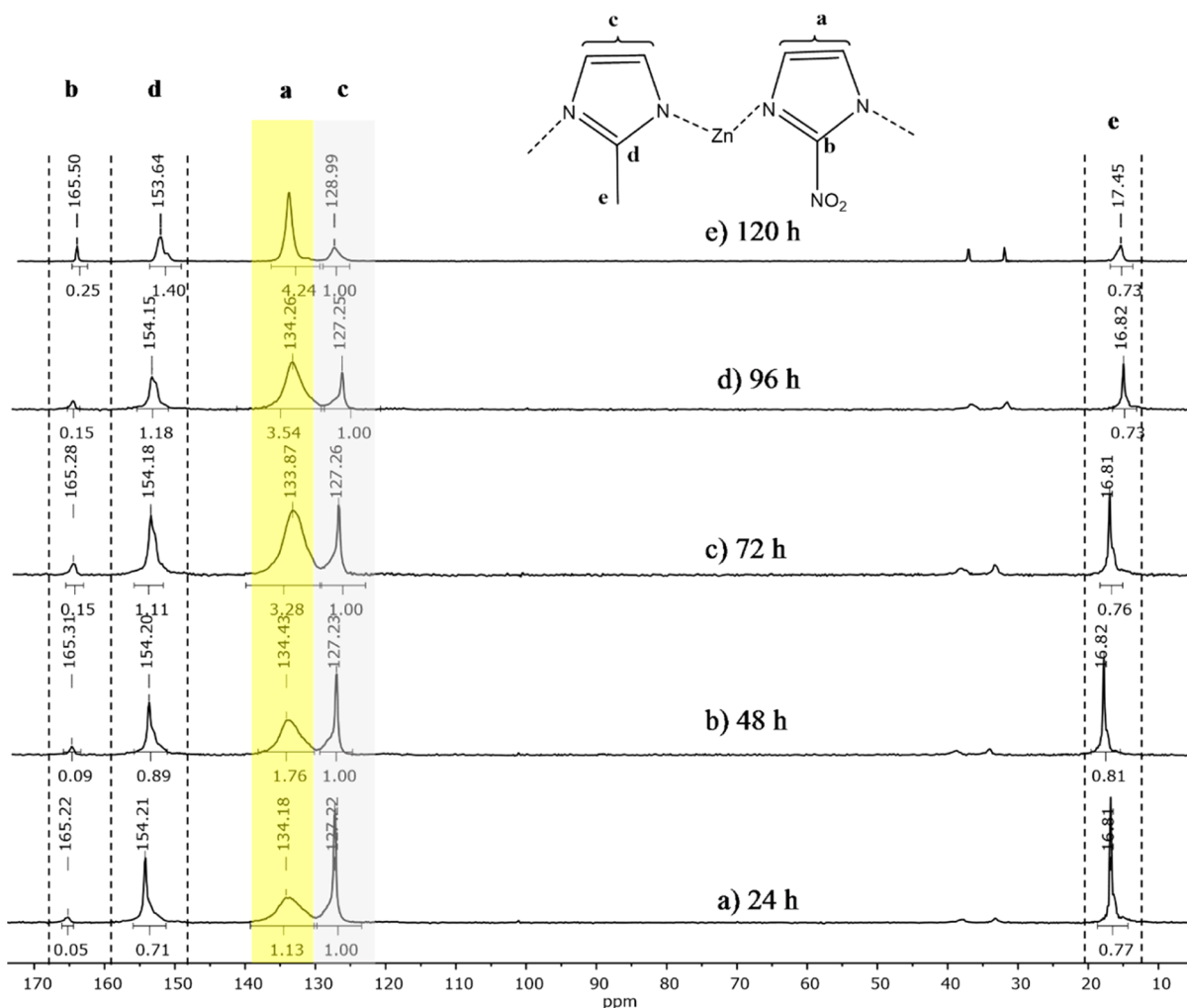


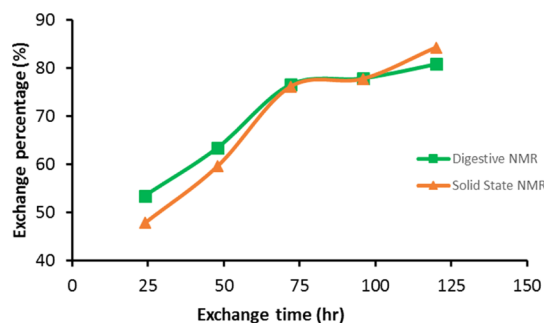
**Figure 2.** Solid-state  $^{13}\text{C}$  NMR Spectra of LeZIF8- $\text{NO}_2\text{Im}$  after (a) 24, (b) 48, (c) 72, (d) 96, and (e) 120 h of ligand exchange.

SHbIm content of 4.25, 6.82, and 9.93% for the 24, 48, and 60 h SALE reactions, respectively (Table 3).

**2.2.2. Solid-State  $^{13}\text{C}$  NMR.** Solid-state  $^{13}\text{C}$  NMR for LeZIF8-BrIm<sub>24h</sub> (19%), LeZIF8-ClIm<sub>24h</sub> (29%), and LeZIF8-CF<sub>3</sub>Im<sub>24h</sub> (4%) (Supporting Information Figure S9) was not useful for quantitative analysis due to their low exchange percentages. The high linker exchange observed for LeZIF8- $\text{NO}_2\text{Im}$  from digestive NMR led to the use of solid-state  $^{13}\text{C}$  NMR to confirm the exchange percentages.

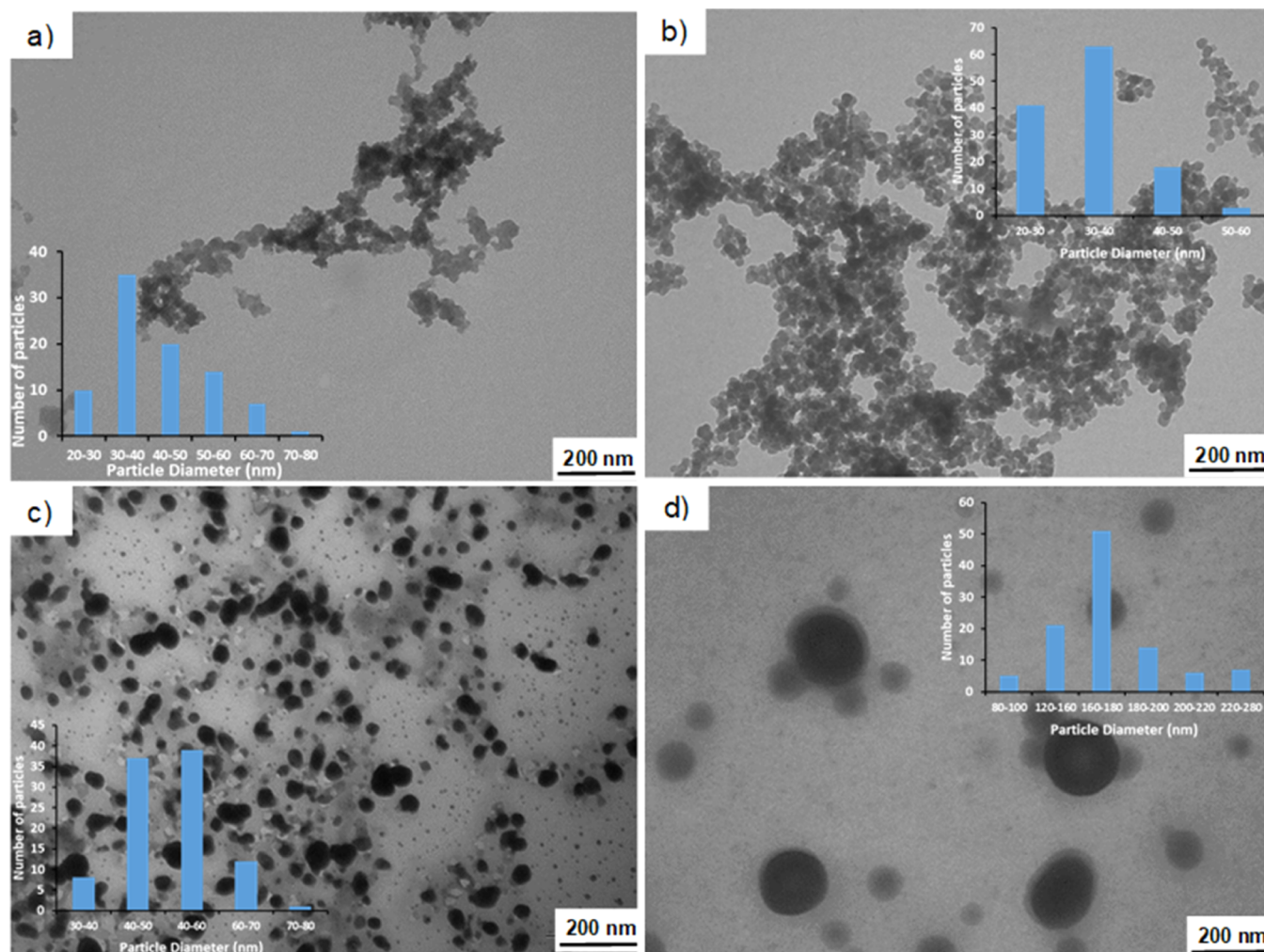
The solid-state  $^{13}\text{C}$  NMR of LeZIF8- $\text{NO}_2\text{Im}$  (Figure 2) have five distinct peaks at 16.8, 127.2, 134.1, 154.2, and 165.5 ppm corresponding to  $\text{CH}_3$  (mIm),  $\text{CH}=\text{CH}$  (mIm),  $\text{CH}=\text{CH}$  ( $\text{NO}_2\text{Im}$ ),  $\text{C}-\text{N}-\text{C}$  (mIm), and  $\text{C}-\text{N}-\text{C}$  ( $\text{NO}_2\text{Im}$ ) carbon atoms, respectively. The exchange percentages were determined from the ratio of  $\text{CH}=\text{CH}$  (mIm) and  $\text{CH}=\text{CH}$  ( $\text{NO}_2\text{Im}$ ) peak intensities/integrals. These exchange percentages are lower by about 10% at low exchange ratios and are similar to those determined from digestive NMR after 72 h of SALE. As with the digestive NMR results, the exchange ratios begin to stabilize after 3 days, reaching a maximum of 81% after 5 days, slightly lower than the 85% determined from digestive  $^1\text{H}$  NMR (Figure 3). Thus, digestive  $^1\text{H}$  NMR is suited for determining low linker exchange rates (<60%), while solid-state  $^{13}\text{C}$  NMR is apt with high linker exchanges.

**2.2.3. PXRD.** The PXRD pattern of all SALE products are identical to the SOD pattern of the synthesized nZIF-8

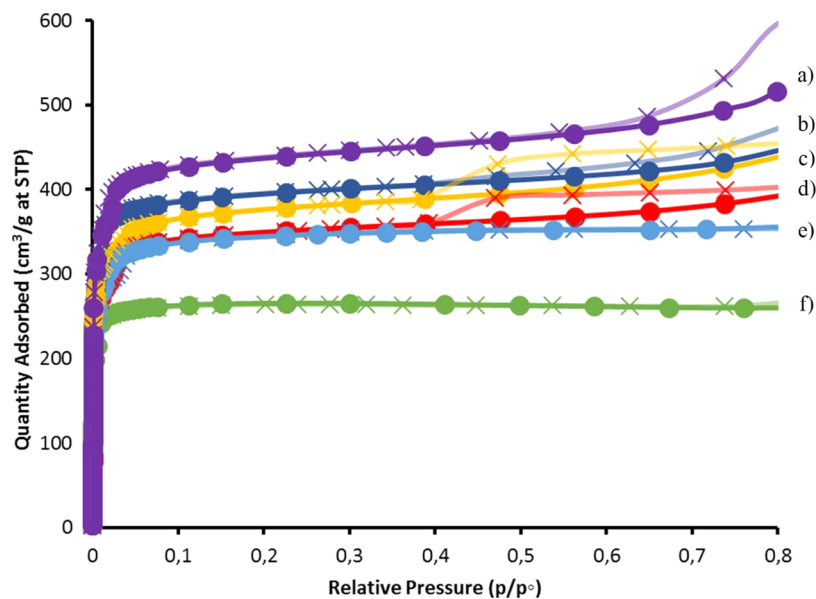


**Figure 3.** Exchange percentages of LeZIF8- $\text{NO}_2\text{Im}$  products determined using digestive  $^1\text{H}$  NMR (■) and solid-state  $^{13}\text{C}$  NMR (▲) as a function of SALE time at 60 °C.

(Supporting Information Figure S3) Thus, the SOD topology of nZIF-8 is maintained during all SALE reactions, as confirmed by the presence of the main peaks of the SOD pattern at  $2\theta = 7.26, 10.18, 12.65,$  and  $17.93^\circ$  for all SALE products. The PXRD patterns also show that the mixed ligand nZIF-8 derivatives are highly crystalline and structurally similar to the mother nZIF-8. The extended SALE time of LeZIF8-SHIm led to a decrease in crystallinity as indicated with the weakening of the peak intensity with increasing SALE time (Supporting Information, Figure S4), confirming the structural



**Figure 4.** TEM images and particle size distribution of (a) LeZIF-8-BrIm<sub>24h</sub> (19%), (b) LeZIF-8-SHIm<sub>60h</sub> (7%), (c) LeZIF-8-ClIm<sub>24h</sub> (29%), and (d) LeZIF-8-NO<sub>2</sub>Im<sub>24h</sub> (54%).

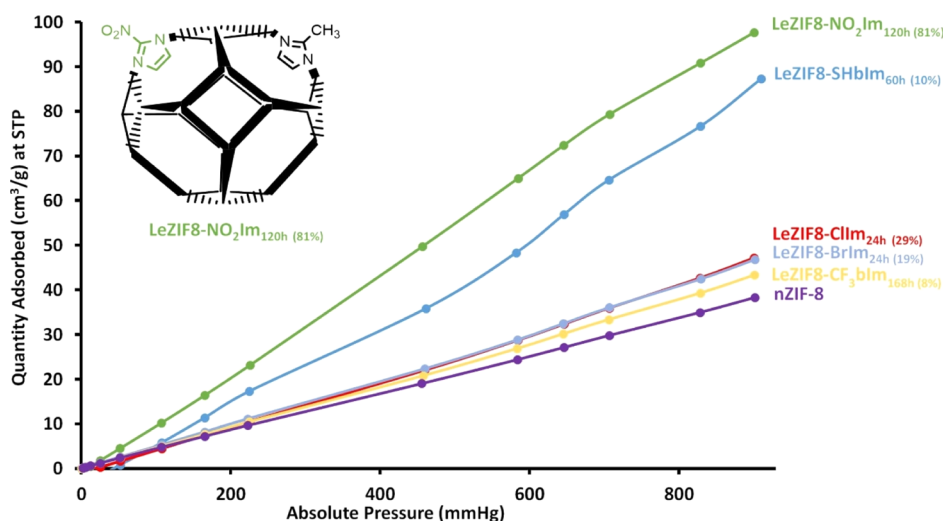


**Figure 5.** N<sub>2</sub> isotherms at 77 K of (a) nZIF-8, (b) LeZIF-8-SHbIm<sub>24h</sub> (2%), (c) LeZIF-8-CF<sub>3</sub>bIm<sub>168h</sub> (8%), (d) LeZIF-8-ClIm<sub>24h</sub> (29%), (e) LeZIF-8-BrIm<sub>24h</sub> (19%), and (f) LeZIF-8-NO<sub>2</sub>Im<sub>24h</sub> (54%). (● = adsorption and × = desorption cycle).

**Table 1. Porosity Analysis (BET, *t*-plot, and Micropore Surface Areas as Well as Micropore Volume by N<sub>2</sub> Adsorption at 77 K) and Low-Pressure CO<sub>2</sub> Uptake at 273 K of all ZIF-8 Derivatives**

compound (exchange %)	BET SA (m <sup>2</sup> g <sup>-1</sup> )	<i>t</i> -plot external SA (m <sup>2</sup> g <sup>-1</sup> )	micropore SA (m <sup>2</sup> g <sup>-1</sup> )	micropore volume (cm <sup>3</sup> g <sup>-1</sup> )	CO <sub>2</sub> quantity adsorbed (cm <sup>3</sup> g <sup>-1</sup> )
nZIF-8	1777	268	1504	0.56	38.3
LeZIF8-BrIm <sub>24h</sub> (19%)	1405	144	1261	0.47	46.8
LeZIF8-ClIm <sub>24h</sub> (29%)	1550	121	1428	0.48	47.1
LeZIF8-CF <sub>3</sub> bIm <sub>168h</sub> (8%)	1562	221	1340	0.49	43.3
LeZIF8-SHbIm <sub>24h</sub> (4.3%) <sup>a</sup>	1625	147	1478	0.49	50.5
LeZIF8-SHbIm <sub>48h</sub> (6.8%) <sup>a</sup>	1655	190	1464	0.53	61.3
LeZIF8-SHbIm <sub>60h</sub> (9.9%) <sup>a</sup>	1693	214	1479	0.58	87.3
LeZIF8-NO <sub>2</sub> Im <sub>24h</sub> (54%)	1161	107	1054	0.37	76.9
LeZIF8-NO <sub>2</sub> Im <sub>48h</sub> (64%)	1285	101	1184	0.45	78.7
LeZIF8-NO <sub>2</sub> Im <sub>72h</sub> (77%)	860	92	768	0.30	86.0
LeZIF8-NO <sub>2</sub> Im <sub>96h</sub> (78%)	897	84	812	0.31	88.8
LeZIF8-NO <sub>2</sub> Im <sub>120h</sub> (81%)	1228	83	1145	0.43	97.6

<sup>a</sup>Exchange percentages from ICP-OES measurements.

**Figure 6.** CO<sub>2</sub> Isotherms, acquired at 273 K and low pressure, for nZIF-8 and the ligand exchanged versions of ZIF-8.

degradation of the MOF due to the acidic thiol substituent. SALE times longer than 60 h was thus not pursued in the case of 2-mercaptobenzimidazole. PXRD patterns of LeZIF8-NO<sub>2</sub>Im SALE products with up to 80% (or 4 days of SALE) linker exchanges showed similar intensities and thus crystallinity to that of nZIF-8 (Supporting Information, Figure S5a–d). Longer (5 days) SALE with NO<sub>2</sub>Im resulted in stronger PXRD peak intensities indicating an improved product crystallinity (Supporting Information, Figure S5e).

**2.2.4. Transmission Electron Microscopy.** The average size of the synthesized ZIF-8 starting material was determined to be 25 nm with a range of 15–34 nm from transmission electron microscopy (TEM) images. TEM images of all SALE products show that the spherical shape of nZIF-8 is maintained, consistent with the SOD topology of the mixed-linker ZIFs (Supporting Information Figure S2). TEM images of SALE products with ClIm, BrIm, CF<sub>3</sub>bIm, and SHbIm linkers showed a slight increase in the particle size, with average sizes between 38 and 51 nm (Figure 4a–c). The bulky CF<sub>3</sub>bIm- and SHbIm-exchanged SALE products did not result in a noticeable increase due to low linker exchange percentages attained. The nitro-functionalized SALE products showed a dramatic size increase, with an average of 148 nm after 24 h of SALE (Figure 4d). The large particle size can be attributed to

the high linker exchange (55%), determined from solid-state <sup>13</sup>C NMR. The general increase in the particle size of the mixed-linker ZIFs can be attributed to the formation of core–shell morphologies, where the SALE starts from the external surface of the MOF.<sup>23</sup>

**2.2.5. Porosity Analyses.** Porosity studies on all activated mixed-linker SALE products with N<sub>2</sub> at 77 K gave typical type-I isotherms, retaining the microporosity of nZIF-8 (Table 1, Figure 5). Application of SALE generally resulted in decreased porosity compared to that of nZIF-8. LeSHbIm SALE products resulted in the highest BET surface areas (1625–1693 m<sup>2</sup> g<sup>-1</sup>), despite the low yields (Table 1, Supporting Information Figure S11). Moreover, increased SALE time with SHbIm led to improved porosity and external surface area, attaining slightly lower BET surface area (1693 m<sup>2</sup> g<sup>-1</sup>) than that of nZIF-8 after 60 h of exchange (9.93%).

The BrIm, ClIm, and CF<sub>3</sub>bIm exchanged SALE products indicated relatively low BET surface areas of 1405, 1450, and 1525 m<sup>2</sup> g<sup>-1</sup>, respectively, compared to that of nZIF-8 starting material. The *t*-plot external surface area of the halogenated SALE products increased with decreasing particle size as determined from TEM images (Table 1, Figure 5c–e). LeZIF8-CF<sub>3</sub>bIm<sub>168h</sub> (8%) with an average size of 38 nm attained an external surface area of 221 m<sup>2</sup> g<sup>-1</sup>. Noticeable hysteresis

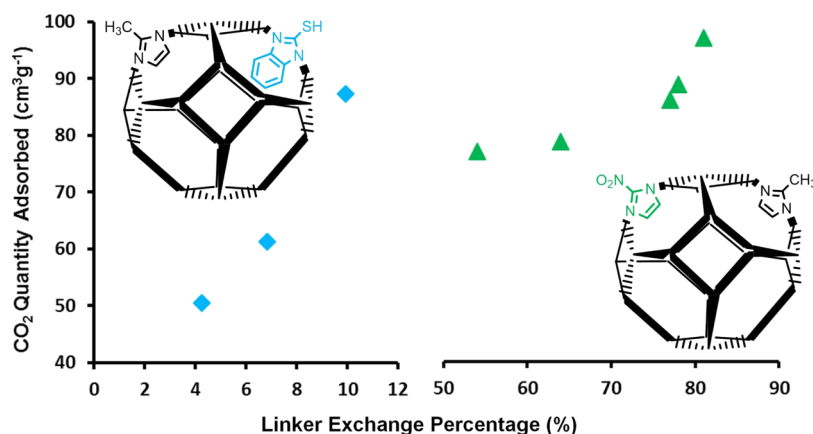


Figure 7. CO<sub>2</sub> adsorption as a function of the linker exchange percentage for NO<sub>2</sub>Im- and SHbIm-exchanged SALE products.

Table 2. CO<sub>2</sub> Uptake of Selected ZIFs and ZIF-8 Derivatives

name	formula	topology	CO <sub>2</sub> uptake (cm <sup>3</sup> g <sup>-1</sup> )	analysis condition	refs
ZIF-8	Zn(mIm) <sub>2</sub>	SOD	38.5	1.2 bar, 273K	22
ZIF-68	Zn(bIm)(NO <sub>2</sub> Im)	GME	65.0	1 bar, 273 K	19
ZIF-69	Zn(5-ClbIm)(NO <sub>2</sub> Im)	GME	69.0	1 bar, 273 K	19
ZIF-70	Zn(Im) <sub>1.13</sub> (NO <sub>2</sub> Im) <sub>0.87</sub>	GME	55.0	1 bar, 273 K	20
ZIF-78	Zn(NO <sub>2</sub> bIm)(NO <sub>2</sub> Im)	GME	68.1	1 bar, 273 K	17
ZIF-79	Zn(mbIm)(NO <sub>2</sub> Im)	GME	34.0	1 bar, 273 K	17
ZIF-81	Zn(brbIm)(NO <sub>2</sub> Im)	GME	66.7	1 bar, 273 K	17
ZIF-82	Zn(CNIm)(NO <sub>2</sub> Im)	GME	85.1	1 bar, 273 K	17
ZIF-108	Zn(NO <sub>2</sub> Im) <sub>2</sub>	SOD	53.0	1 bar, 273 K	25
LeZIF8-NO <sub>2</sub> Im <sub>168h</sub>	Zn(mIm) <sub>0.67</sub> (NO <sub>2</sub> Im) <sub>1.33</sub>	FRL	76.0	1.2 bar, 273K	22
LeZIF8-SHBzIm <sub>72h</sub>	Zn(mIm) <sub>1.76</sub> (SHbIm) <sub>0.24</sub>	SOD	77.2	1.2 bar, 273K	22
LeZIF8-PhIm	Zn(mIm) <sub>1.8</sub> (PhIm) <sub>0.2</sub>	SOD	49.9	1.2 bar, 273K	22
LeZIF8-NH <sub>2</sub> BzIm	Zn(mIm) <sub>1.8</sub> (NH <sub>2</sub> bIm) <sub>0.2</sub>	SOD	48.2	1.2 bar, 273K	22
LeZIF8-ClIm <sub>24h</sub> (29%)	Zn(mIm) <sub>1.42</sub> (ClIm) <sub>0.58</sub>	SOD	47.1	1.2 bar, 273K	<sup>a</sup>
LeZIF8-BrIm <sub>24h</sub> (19%)	Zn(mIm) <sub>1.62</sub> (BrIm) <sub>0.38</sub>	SOD	46.8	1.2 bar, 273K	<sup>a</sup>
LeZIF8-CF <sub>3</sub> BzIm <sub>168h</sub> (8%)	Zn(mIm) <sub>1.76</sub> (CF <sub>3</sub> bIm) <sub>0.24</sub>	SOD	43.3	1.2 bar, 273K	<sup>a</sup>
LeZIF8-SHBzIm <sub>60h</sub> (7%)	Zn(mIm) <sub>1.86</sub> (SHbIm) <sub>0.14</sub>	SOD	87.3	1.2 bar, 273K	<sup>a</sup>
LeZIF8-NO <sub>2</sub> Im <sub>120h</sub> (81%)	Zn(mIm) <sub>0.38</sub> (NO <sub>2</sub> Im) <sub>1.62</sub>	SOD	97.6	1.2 bar, 273K	<sup>a</sup>

<sup>a</sup>This work.

loops are observed with the desorption cycle of LeZIF8-ClIm<sub>24h</sub> (29%) and LeZIF8-CF<sub>3</sub>bIm<sub>168h</sub> (8%) due to capillary condensation.

LeNO<sub>2</sub>Im SALE products resulted in the most drastic drop in porosity due to the high (54–81%) linker exchange with NO<sub>2</sub>Im (Table 1, Supporting Information Figure S12). Time-resolved SALE study showed a drop in porosity for the first 3 days of SALE reactions, with LeNO<sub>2</sub>Im<sub>72h</sub> (77%) reaching a low BET surface area of 860 m<sup>2</sup> g<sup>-1</sup> with a micropore volume of 0.3 cm<sup>3</sup> g<sup>-1</sup>. Longer SALE reactions led to improved porosity results, with LeNO<sub>2</sub>Im<sub>120h</sub> (81%) recording the highest porosity of the NO<sub>2</sub>Im SALE series with a BET surface area of 1228 m<sup>2</sup> g<sup>-1</sup> and a micropore volume of 0.43 cm<sup>3</sup> g<sup>-1</sup>, respectively. This is consistent with the observed improvements in the crystallinity of LeNO<sub>2</sub>Im<sub>120h</sub> (81%) (Supporting Information, Figure S5e). LeNO<sub>2</sub>Im SALE products also showed the least external surface area, in line with the large particle size observed in TEM images (Figure 4).

**2.2.6. CO<sub>2</sub> Adsorption.** Carbon dioxide adsorption of mixed-linker ZIFs (SALE products) were measured at 273 K under low-pressure conditions (0–1 bar) and compared to the CO<sub>2</sub> capacity of synthesized nZIF-8 (38.3 cm<sup>3</sup> g<sup>-1</sup>) (Figure 6 and Table 1). The -Cl- and -Br-functionalized SALE

products showed slight improvements with CO<sub>2</sub> adsorptions of 46.8 and 47.1 cm<sup>3</sup> g<sup>-1</sup>, respectively. This corresponds well with the marginally higher electronegativity of the Cl substituent, along with the higher linker exchange of 29% attained compared to 19% of LeZIF8-BrIm<sub>24h</sub> (19%). LeZIF8-CF<sub>3</sub>bIm<sub>24h</sub> (4%) showed the least improvement of all SALE products with regard to CO<sub>2</sub> uptake, despite the high electronegativity of the CF<sub>3</sub> group. This was initially ascribed to the low linker exchange (4%) since exchange of the bulky CF<sub>3</sub>bIm linker was limited to the external surface of nZIF-8. However, extended (168 h) SALE with CF<sub>3</sub>bIm resulted in nearly double the exchange percentage achieved after 24 h, but it did not yield any significant improvement of CO<sub>2</sub> uptake. Thus, the application of SALE with electron-withdrawing CF<sub>3</sub>bIm is not effective in increasing the CO<sub>2</sub> uptake of nZIF-8.

LeZIF8-SHBzIm<sub>24h</sub> with only 4.25% linker exchange attained a high CO<sub>2</sub> uptake of 51.5 cm<sup>3</sup> g<sup>-1</sup>. A time study (24–60 h) of this SALE resulted in a nearly linear increase of CO<sub>2</sub> adsorption with increasing SALE time (Figure 7). A maximum CO<sub>2</sub> uptake of 87.3 cm<sup>3</sup> g<sup>-1</sup> was achieved after 60 h of SALE with a low linker exchange of 9.93%. Longer SALE reactions

were not ideal since the acidic nature of the SHbIm linker resulted in structural degradation of the MOF and low yields.<sup>22</sup>

LeZIF8-NO<sub>2</sub>Im<sub>24h</sub> shows the highest improvement of all SALE products after 24 h of SALE, with a CO<sub>2</sub> uptake of 76.9 cm<sup>3</sup> g<sup>-1</sup>. This is even more remarkable, given its lower BET surface area (1161 m<sup>2</sup> g<sup>-1</sup>) and external surface area (107 m<sup>2</sup> g<sup>-1</sup>) compared to all other SALE products. A time-resolved study (24–120 h) SALE of nZIF-8 with NO<sub>2</sub>Im shows that CO<sub>2</sub> uptake increases linearly with reaction time and linker exchange percentage, reaching a maximum of 97.6 cm<sup>3</sup> g<sup>-1</sup> after 120 h (Figure 6, Table 1). This is almost a threefold increase in CO<sub>2</sub> adsorptions of the unmodified nZIF-8 and the highest CO<sub>2</sub> uptake of all reported ZIF derivatives at low-pressure conditions, surpassing the 85 cm<sup>3</sup> g<sup>-1</sup> attained by ZIF-82 (with NO<sub>2</sub>Im and CNIm linkers) (Figure 6 and Table 2).

The CO<sub>2</sub> uptakes of the mixed-linker products show that enhanced adsorptions are more dependent on the functionality of the linker rather than the surface area (BET and *t*-plot external surface area) of the MOF. The enhanced CO<sub>2</sub> uptakes of the SALE products can be attributed to the electron-withdrawing groups (EWGs)/functionality of the newly introduced linkers. EWG increases the electrostatic/Van der Waal interactions between the ZIF and CO<sub>2</sub> molecules, where the locally diminished electron density causes the slightly polar CO<sub>2</sub> molecules to be attracted by the MOF.<sup>2</sup> LeZIF-8NO<sub>2</sub>Im results in an additional Lewis acid–base interaction between CO<sub>2</sub> and the nitro group, leading to further enhancement in CO<sub>2</sub> uptakes. The dramatic CO<sub>2</sub> uptakes of LeZIF8-SHbIm is due to the enhanced binding of CO<sub>2</sub> molecules to the thiol functional groups and lower adsorption energies of SH containing ZIF unit cells, as shown by the theoretical work done by Bolotov *et al.* and Tsai *et al.*, respectively.<sup>18,24</sup>

## 4. CONCLUSIONS

ZIF-8 is a potent CO<sub>2</sub> absorbent, whose absorption capacity for CO<sub>2</sub> can be increased by a factor of up to 2.5 by postsynthetically replacing more than 80% of its 2-methylimidazolate ligands by 2-nitroimidazolate using a method called SALE.

Functionalized imidazoles such as 2-nitroimidazole (NO<sub>2</sub>Im), 2-chloroimidazole (ClIm), 2-bromoimidazole (BrIm), 2-trifluoromethylbenzimidazole (CF<sub>3</sub>bIm), and 2-mercaptobenzimidazole (SHbIm) were successfully incorporated in the nZIF-8 structure *via* SALE while maintaining the SOD topology of nZIF-8. Linker exchange percentages were controlled by the synthesis time and determined *via* digestive <sup>1</sup>H NMR and solid-state <sup>13</sup>C NMR.

All mixed-linker nZIF-8 SALE products had improved CO<sub>2</sub> uptake when compared to nZIF-8. The halogenated (–Cl, –Br, and –CF<sub>3</sub>) imidazolate linkers resulted in moderate (11–22%) improvement in CO<sub>2</sub> uptake, while SALE with 2-mercapto-benzimidazole (SHbIm) and 2-nitroimidazole (NO<sub>2</sub>Im) improved the CO<sub>2</sub> uptake with up to 128 and 155%. The latter is so far the highest of all reported low pressure CO<sub>2</sub> uptakes by a ZIF derivative.

## 5. EXPERIMENTAL SECTION

**5.1. Materials and Equipment.** All chemical reagents were purchased from Sigma-Aldrich, with the exception of 2-nitroimidazole, which was obtained from Ambeed, USA. All solvents were purchased from Merck. Chemicals and solvents were used without further purification, unless stated otherwise.

PXRD patterns were collected on a Bruker D2 PHASER powder X-ray diffractometer at room temperature, employing a flat plate sample holder and Cu radiation ( $\lambda = 1.54 \text{ \AA}$ ). Diffraction patterns were collected in the range 5–50° for 2 $\theta$ , with a step size of 0.1° and a counting time of 2 s per step. <sup>1</sup>H NMR spectra were measured on a 300 MHz Bruker Fourier NMR spectrometer with a 5 mm <sup>13</sup>C/<sup>1</sup>H high-resolution NMR probe equipped with a Z gradient coil. The <sup>1</sup>H chemical shifts are reported relative to SiMe<sub>4</sub> at 0.0 ppm as the external standard and utilizing the solvent peak as the internal standard, where applicable. Soluble compounds were dissolved in dimethyl sulfoxide, unless stated otherwise. <sup>13</sup>C Solid-state NMR spectra were measured on a Bruker 400 MHz AVANCE III NMR spectrometer with a 4 mm VTN multinuclear double-resonance-magic-angle spinning probe operating at 25 °C having a <sup>13</sup>C frequency of 100.61 MHz. All infrared spectra were measured on a Thermo Scientific Nicolet iS50 ATR infrared spectrometer with OMNIC v9.2.86 software from 500–4000 cm<sup>-1</sup>. Shimadzu ICPS-7510 ICP–optical emission spectrometry (ICP-OES) with a radial-sequential plasma spectrometer was used for the wet chemical analysis. TGA were performed on a METTLER TOLEDO TGA/SDTA851 analyzer under an N<sub>2</sub> atmosphere, and the data were analyzed with METTLER STARe Evaluation software.

All porosity and surface area measurements were performed on a Micromeritics ASAP 2020 surface area and porosity analyzer, and the data were analyzed with ASAP 2020 V2.0 for physisorption with nitrogen and carbon dioxide. Nitrogen adsorption was measured with a relative pressure at 77 K, and carbon dioxide was measured with an absolute pressure at 273 K. A typical amount of ~40 mg was used for each analysis with the warm and cold free space determined separately with helium. Porosity results were refined by MicroActive V1.01 software. TEM was performed with a Philips (FEI) CM100 equipped with a MegaView III digital camera. TEM pictures were analyzed utilizing Soft Imaging System (analySIS) software.

**5.2. Synthesis of ZIF-8 Nanoparticles.** nZIF-8 was synthesized using an adopted procedure from the literature.<sup>26</sup> Zn(NO<sub>3</sub>)<sub>2</sub>·4H<sub>2</sub>O (1.3050 g, 5 mmol) was dissolved in methanol (150 cm<sup>3</sup>) and heated to 60 °C with stirring. This solution was rapidly added to a solution of 2-methylimidazole (3.284 g, 40 mmol) that was dissolved in methanol (150 cm<sup>3</sup>) and heated to 60 °C. The resulting solution slowly turned milky and was stirred for 1 h at 60 °C. The formed nZIF-8 nanocrystals were then isolated by centrifugation (8500 rpm, 30 min, 15 °C), washed with methanol (3 × 150 cm<sup>3</sup>), and isolated by centrifugation. The product was dried overnight and activated in vacuum at 150 °C to yield nano-ZIF-8 as a white powder (0.5715 g, 44.7%).

**5.3. SALE of ZIF-8.** A general SALE procedure was adopted from the literature.<sup>22</sup> nZIF-8 (0.300 g, 1.306 mmol) was suspended in solvent I (30 cm<sup>3</sup>) with an ultrasonic probe for 3 min and transferred into a Teflon cup in a stainless steel reactor. Consequently, the functionalized imidazole was then dissolved in solvent II (30 cm<sup>3</sup>) and mixed with the nZIF-8 suspension. The reactor was sealed and heated to the desired temperature for a set time. After cooling, the nanocrystals were isolated by centrifugation (8500 rpm, 30 min, 15 °C) and washed with methanol (3 × 100 cm<sup>3</sup>) and DMF (2 × 100 cm<sup>3</sup>) for 2-nitroimidazole SALE products. The mixed-linker nZIF-8 derivative was then air dried overnight and activated in vacuum at 150 °C. Yields and reaction conditions for the SALE

**Table 3. SALE Reaction Conditions, Product Yields, and Linker Exchange Percentages (Determined by Digestive <sup>1</sup>H NMR and ICP-OES\* for the SHbIm Linker)**

imidazole derivative	reaction time (h)	temp (°C)	solvent I	solvent II	yield (%)	linker exchange (%)
2-mercapto-benzimidazole (SHbIm)	24	100	<i>n</i> -butanol	<i>n</i> -butanol	32	2 (4.25*)
	48				27	6 (6.82*)
	60				30	7 (9.93*)
2-chloroimidazole (ClIm)	24	60	methanol	methanol	97	29
2-bromoimidazole (BrIm)	24	60	methanol	methanol	95	19
2-trifluoromethyl-benzimidazole (CF <sub>3</sub> BIm)	24	60	methanol	methanol	82	4
	168				84	7
2-nitroimidazole (NO <sub>2</sub> Im)	24	60	methanol	DMF	83	54
	48				83	64
	72				90	77
	96				79	78
	120				80	81

procedures are summarized in Table 3, and Scheme 1 presents an overview of all systems prepared.

## ■ ASSOCIATED CONTENT

### SI Supporting Information

The Supporting Information is available free of charge at <https://pubs.acs.org/doi/10.1021/acsomega.1c01130>.

List of all reported CO<sub>2</sub> uptakes of ZIF derivatives to date; FTIR spectra; PXRD patterns; digestive <sup>1</sup>H NMR; solid-state <sup>13</sup>C NMR; TGA thermograms; N<sub>2</sub> and CO<sub>2</sub> isotherms of nZIF-8; and SALE products (PDF)

## ■ AUTHOR INFORMATION

### Corresponding Author

Ernst H. G. Langner – Department of Chemistry, University of the Free State, Bloemfontein 9300, South Africa; [orcid.org/0000-0002-4667-3396](https://orcid.org/0000-0002-4667-3396); Email: [langneeh@ufs.ac.za](mailto:langneeh@ufs.ac.za)

### Authors

Yuel W. Abraha – Department of Chemistry, University of the Free State, Bloemfontein 9300, South Africa; [orcid.org/0000-0002-3633-1835](https://orcid.org/0000-0002-3633-1835)

Chih-Wei Tsai – Department of Chemistry, University of the Free State, Bloemfontein 9300, South Africa; Department of Physics, University of the Free State, Bloemfontein 9300, South Africa

J. W. Hans Niemantsverdriet – [SynCat@DIFFER](mailto:SynCat@DIFFER), Syngaschem BV, 5600 HH Eindhoven, The Netherlands

Complete contact information is available at: <https://pubs.acs.org/doi/10.1021/acsomega.1c01130>

### Notes

The authors declare no competing financial interest.  
\*Email (J.W.H.N.): [jwn@syngaschem.com](mailto:jwn@syngaschem.com).

## ■ ACKNOWLEDGMENTS

This work was financially supported by the National Nanoscience Postgraduate Teaching and Training Programme (NNPTTP), South Africa, the National Research Foundation of South Africa (grant no: 121540), and Syngaschem BV, Netherlands, which acknowledges substantial funding by Syngaschem China Technology Co., Ltd.

## ■ REFERENCES

- Modak, A.; Subhra, J. Advances in Porous Adsorbents for CO<sub>2</sub> Capture and Storage. *Carbon Dioxide Chemistry, Capture and Oil Recovery*; IntechOpen, 2017; Vol. 1, pp 166–183.
- Marti, A. M. Metal–Organic Frameworks Materials for Post-Combustion CO<sub>2</sub> Capture. *Materials and Processes for CO<sub>2</sub> Capture, Conversion, and Sequestration*; John Wiley & Sons, Inc, 2014; pp 84–94.
- Sumida, K.; Rogow, D. L.; Mason, J. A.; McDonald, T. M.; Bloch, E. D.; Herm, Z. R.; Bae, T.-H.; Long, J. R. Carbon Dioxide Capture in Metal–Organic Frameworks. *Chem. Rev.* **2011**, *112*, 724–781.
- Kenarsari, S. D.; Yang, D.; Jiang, G.; Zhang, S.; Wang, J.; Russell, A. G.; Wei, Q.; Fan, M. Review of Recent Advances in Carbon Dioxide Separation and Capture. *RSC Adv.* **2013**, *3*, 22739–22773.
- Bae, Y.-S.; Snurr, R. Q. Development and Evaluation of Porous Materials for Carbon Dioxide Separation and Capture. *Angew. Chem. Int. Ed.* **2011**, *50*, 11586–11596.
- Keskin, S.; van Heest, T. M.; Sholl, D. S. Can Metal-Organic Framework Materials Play a Useful Role in Large-Scale Carbon Dioxide Separations? *ChemSusChem* **2010**, *3*, 879–891.
- Küsgens, P.; Rose, M.; Senkowska, I.; Fröde, H.; Henschel, A.; Siegle, S.; Kaskel, S. Characterization of Metal-Organic Frameworks by Water Adsorption. *Microporous Mesoporous Mater.* **2009**, *120*, 325–330.
- Tuleushov, G.; Attfield, M. Synthesis of Metal Organic Framework Materials by Performing Linker Exchanges Using Solvothermal Procedure. *Int. J. Biol. Chem.* **2018**, *11*, 198–202.
- Karagiari, O.; Bury, W.; Mondloch, J. E.; Hupp, J. T.; Farha, O. K. Solvent-Assisted Linker Exchange: An Alternative to the de Novo Synthesis of Unattainable Metal-Organic Frameworks. *Angew. Chem. Int. Ed.* **2014**, *53*, 4530–4540.
- Deria, P.; Mondloch, J. E.; Karagiari, O.; Bury, W.; Hupp, J. T.; Farha, O. K. Beyond Post-Synthesis Modification: Evolution of Metal-Organic Frameworks via Building Block Replacement. *Chem. Soc. Rev.* **2014**, *43*, 5896–5912.
- Karagiari, O.; Bury, W.; Sarjeant, A. A.; Stern, C. L.; Farha, O. K.; Hupp, J. T. Synthesis and Characterization of Isostructural Cadmium Zeolitic Imidazolate Frameworks via Solvent-Assisted Linker Exchange. *Chem. Sci.* **2012**, *3*, 3256–3260.
- Lalonde, M. B.; Mondloch, J. E.; Deria, P.; Sarjeant, A. A.; Al-Juaid, S. S.; Osman, O. I.; Farha, O. K.; Hupp, J. T. Selective Solvent-Assisted Linker Exchange (SALE) in a Series of Zeolitic Imidazolate Frameworks. *Inorg. Chem.* **2015**, *54*, 7142–7144.
- Kim, M.; Cahill, J. F.; Fei, H.; Prather, K. A.; Cohen, S. M. Postsynthetic Ligand and Cation Exchange in Robust Metal-Organic Frameworks. *J. Am. Chem. Soc.* **2012**, *134*, 18082–18088.
- Fei, H.; Cahill, J. F.; Prather, K. A.; Cohen, S. M. Tandem Postsynthetic Metal Ion and Ligand Exchange in Zeolitic Imidazolate Frameworks. *Inorg. Chem.* **2013**, *52*, 4011–4016.

(15) Ban, Y.; Peng, Y.; Yang, W.; Zhang, Y.; Wang, P.; Jin, H.; Guo, A.; Li, Y.; Jiao, W. Dual-Ligand Zeolitic Imidazolate Framework Crystals and Oriented Films Derived from Metastable Mono-Ligand ZIF-108. *Microporous Mesoporous Mater.* **2016**, *219*, 190–198.

(16) Deria, P.; Mondloch, J. E.; Tylianakis, E.; Ghosh, P.; Bury, W.; Snurr, R. Q.; Hupp, J. T.; Farha, O. K. Perfluoroalkane Functionalization of NU-1000 via Solvent-Assisted Ligand Incorporation: Synthesis and CO<sub>2</sub> Adsorption Studies Table of Contents. *J. Am. Chem. Soc.* **2013**, *135*, 16801–16804.

(17) Wang, B.; Côté, A. P.; Furukawa, H.; O’Keeffe, M.; Yaghi, O. M. Colossal Cages in Zeolitic Imidazolate Frameworks as Selective Carbon Dioxide Reservoirs. *Nature* **2008**, *453*, 207–211.

(18) Tsai, C.-W.; Langner, E. H. G.; Harris, R. A. Computational Study of ZIF-8 Analogues with Electron Donating and Withdrawing Groups for CO<sub>2</sub> Adsorption. *Microporous Mesoporous Mater.* **2019**, *288*, 109613.

(19) Banerjee, R.; Phan, A.; Wang, B.; Knobler, C.; Furukawa, H.; O’Keeffe, M.; Yaghi, O. M. High-Throughput Synthesis of Zeolitic Imidazolate Frameworks and Application to CO<sub>2</sub> Capture. *Science* **2008**, *319*, 939–943.

(20) Phan, A.; Doonan, C. J.; Uribe-Romo, F. J.; Knobler, C. B.; O’Keeffe, M.; Yaghi, O. M. Synthesis, Structure, and Carbon Dioxide Capture Properties of Zeolitic Imidazolate Frameworks. *Acc. Chem. Res.* **2010**, *43*, 58–67.

(21) Abbasi, A. R.; Moshtkob, A.; Shahabadi, N.; Yaser Masoomi, M.; Morsali, A. Synthesis of Nano Zinc-Based Metal–Organic Frameworks under Ultrasound Irradiation in Comparison with Solvent-Assisted Linker Exchange: Increased Storage of N<sub>2</sub> and CO<sub>2</sub>. *Ultrason. Sonochem.* **2019**, *59*, 104729.

(22) Tsai, C.-W.; Niemantsverdriet, J. W.; Langner, E. H. G. Enhanced CO<sub>2</sub> Adsorption in Nano-ZIF-8 Modified by Solvent Assisted Ligand Exchange. *Microporous Mesoporous Mater.* **2018**, *262*, 98–105.

(23) Jayachandrababu, K. C.; Sholl, D. S.; Nair, S. Structural and Mechanistic Differences in Mixed-Linker Zeolitic Imidazolate Framework Synthesis by Solvent Assisted Linker Exchange and de Novo Routes. *J. Am. Chem. Soc.* **2017**, *139*, 5906–5915.

(24) Bolotov, V. A.; Kovalenko, K. A.; Samsonenko, D. G.; Han, X.; Zhang, X.; Smith, G. L.; McCormick, L. J.; Teat, S. J.; Yang, S.; Lennox, M. J.; Henley, A.; Besley, E.; Fedin, V. P.; Dybtsev, D. N.; Schröder, M. Enhancement of CO<sub>2</sub> Uptake and Selectivity in a Metal–Organic Framework by the Incorporation of Thiophene Functionality. *Inorg. Chem.* **2018**, *57*, 5074–5082.

(25) Ban, Y.; Li, Y.; Peng, Y.; Jin, H.; Jiao, W.; Liu, X.; Yang, W. Metal-Substituted Zeolitic Imidazolate Framework ZIF-108: Gas-Sorption and Membrane-Separation Properties. *Chem.—Eur. J.* **2014**, *20*, 11402–11409.

(26) Tsai, C.-W.; Langner, E. H. G. The Effect of Synthesis Temperature on the Particle Size of Nano-ZIF-8. *Microporous Mesoporous Mater.* **2016**, *221*, 8–13.

## NOTE ADDED AFTER ISSUE PUBLICATION

The affiliation for J. W. Hans Niemantsverdriet was changed to reflect where the work was done. The original version of the paper was published on August 18, 2021. The revised version was published on September 24, 2021.